Queensland University of Technology
Brisbane Australia

This is the author's version of a work that was submitted/accepted for publication in the following source:

Tesfamichael, T., Ahsan, M., Notarianni, M., Groß, A., Hagen, G., Moos, R., Ionescu, M., & Bell, J.
(2014)
Gas sensing of ruthenium implanted tungsten oxide thin films.
Thin Solid Films, *558*, pp. 416-422.

This file was downloaded from: http://eprints.qut.edu.au/69947/

© Copyright 2014 2014 Elsevier B.V. All rights reserved.

This is the author's version of a work that was accepted for publication in Thin Solid Films. Changes resulting from the publishing process, such as peer review, editing, corrections, structural formatting, and other quality control mechanisms may not be reflected in this document. Changes may have been made to this work since it was submitted for publication. A definitive version was subsequently published in Thin Solid Films, [in press] DOI: 10.1016/j.tsf.2014.02.084

Notice: *Changes introduced as a result of publishing processes such as copy-editing and formatting may not be reflected in this document. For a definitive version of this work, please refer to the published source:*

http://doi.org/10.1016/j.tsf.2014.02.084

Thin Solid Films; In Press Available online 11 March 2014,
http://dx.doi.org/10.1016/j.tsf.2014.02.084

Gas Sensing of Ruthenium Implanted Tungsten Oxide Thin Films

[a,*]T. Tesfamichael, [b]M. Ahsan, [a]M. Notarianni, [c]A. Groß, [c]G. Hagen, [c]R. Moos, [d]M. Ionescu, [a]J. Bell

[a] Institute for Future Environments and School of Chemistry, Physics and Mechanical Engineering, Queensland University of Technology, 2 George Street, Brisbane, QLD 4000, Australia

[b] William A. Cook Australia, 95 Brandl Street Eight Mile Plains, Brisbane, QLD 4113, Australia

[c] University of Bayreuth, Faculty of Engineering Science, Department of Functional Materials, Universitätsstr. 30, 95440 Bayreuth, Germany

[d] ANSTO, Institute for Environmental Research, Locked Bag 2001, Kirrawee DC NSW 2232, Australia

*Corresponding Author contacts:
Phone: +61731381988
Fax: +61731384438
email: t.tesfamichael@qut.edu.au

Abstract

Different amounts of Ru were implanted into thermally evaporated WO_3 thin films by ion implantation. The films were subsequently annealed at 600^{o}C for 2 hours in air to remove defects generated during the ion implantation. The Ru concentrations of four samples have been quantified by Rutherford Backscattering Spectrometry as 0.8, 5.5, 9 and 11.5 at%. The un-implanted WO_3 films were highly porous but the porosity decreased significantly after ion implantation as observed by Transmission Electron Microscopy and Scanning Electron Microscopy. The thickness of the films also decreased with increasing Ru-ion dose, which is mainly due to densification of the porous films during ion implantation. From Raman spectroscopy two peaks at 408 and 451 cm^{-1} (in addition to the typical vibrational peaks of the monoclinic WO_3 phase) associated with Ru were observed. Their intensity increased with increasing Ru concentration. X-Ray Photoelectron Spectroscopy showed a metallic state of Ru with binding energy of Ru $3d_{5/2}$ at 280.1 eV. This peak position remained almost unchanged with increasing Ru concentration. The resistances of the Ru-implanted films were found to increase in the presence of NO_2 and NO with higher sensor response to NO_2. The effect of Ru concentration on the sensing performance of the films was not explicitly observed due to reduced film thickness and porosity with increasing Ru concentration. However, the results indicate that the implantation of Ru into WO_3 films with sufficient film porosity and film thickness can be beneficial for NO_2 sensing at temperatures in the range of 250°C to 350°C.

Keywords

Nanostructured tungsten oxide; thin films; Ru-ion implantation; sensor response; NO_2 gas sensors.

1. Introduction

Thin Solid Films; In Press Available online 11 March 2014,
http://dx.doi.org/10.1016/j.tsf.2014.02.084

Transition semiconducting metal oxides such as SnO_2, ZnO, TiO_2, ln_2O_3, Fe_2O_3, WO_3 and MoO_3 have been widely investigated for gas sensing devices because of their simplicity and low cost [1-12]. The most common sensing mechanism of the metal oxide sensors involves the changes in the electrical resistance induced by reactions between the target gas and the film surface [13]. These reactions cause injection or extraction of electrons from the metal oxide, changing the resistance of the material. The semiconducting oxides show good chemo-sensitivity towards oxidizing and reducing gases and have been widely used for sensing various gases and vapors. Key sensor response parameters, characterizing the sensing behavior of the metal oxide sensors, are the sensor response (sometimes denoted as sensitivity), the response and recovery times and the selectivity. The sensor response of n-type semiconducting metal oxides (e.g. WO_3) in oxidizing gases such as NO and NO_2 [12] can be defined as R/R_0; where R_0 and R are the steady state resistance values achieved within reasonable time during the exposure of the sample to the reference gas (synthetic air) and the target gas, respectively. The response (τ_{RESP}) and recovery (τ_{REC}) times are important sensor characteristics. τ_{RESP} is here is defined as the time the sensor resistance takes to reach the 90% of its final value), and τ_{REC} as the time the sensor response takes to recover the 90% of its baseline value. The sensor performance (i.e. sensor response, response time and recovery time) is highly dependent on the film characteristics (electronic properties, crystallinity, grain size, defect structure, vacancies, porosity, film thickness, film stoichiometry, and surface morphology). These factors can be controlled by changing the deposition conditions, the post-deposition annealing, and doping [3; 12; 14; 15].

Thin films of tungsten oxide (WO_3) deposited by Physical Vapor Deposition techniques are very promising for gas sensing due to the intrinsic electronic properties of the material. In fact, tungsten oxide has a good response towards various gases at lower operating temperatures because of a slight substoichiometry [16-19]. The material behaves like an n-type semiconductor because of its non-stoichiometry, predominantly due to defects in oxygen vacancies. As the metal oxide approaches stoichiometry, the conductivity change of the material due to target gas can be very low and hence a reduction of the sensor response is obtained. Sensor response can be enhanced through tailoring and optimizing nanostructural parameters such as particle size, surface morphology, film thickness and porosity. Porous nanostructured materials have a very large surface-to-volume ratio offering more surface/gas interaction and thereby enhance both sensor response and response time significantly [20]. Several theoretical studies [21; 22] have shown that the sensor response can be significantly enhanced if the grain size is smaller than 50 nm as confirmed by previous work [17; 19]. Sensors made of WO_3 nanotubes have also shown enhanced gas response due to the large surface area presented by the interior of the nanotube assemblies [23]. Metal inclusions are important for the formation of oxygen vacancies, modification of the electronic structure, and band gap energy of metal oxides in order to enhance response to target gases [24-26]. In most of the literature, doping concentration has been limited to about 5 wt% [27], but higher values (up to 25 wt%) have been shown to improve the sensing performance [28]. Metal doping can also change the response to specific gases by increasing the sensor response to specific gases (i.e. selectivity) [29]. High response and selectivity of Pd-doped WO_3 films to H_2 gas have

Thin Solid Films; In Press Available online 11 March 2014,
http://dx.doi.org/10.1016/j.tsf.2014.02.084

been reported at working temperature of 200°C [30]. The response of WO_3 film to NO_2 and NH_3 has been improved when doped with Ag and Pt, respectively [31]. Studies have shown that the addition of Cu to WO_3 thin film improved the sensor response when exposed to NO_2 [32], whereas addition of Fe increased the response to ozone, CO and ethanol [33]. It has been reported that doping of TiO_2 film with Fe increased the oxidation activity of the oxide and this has been related to a higher density of oxygen vacancies [28]. Film thickness is another parameter that can have significant effect in optimizing sensor selectivity and response [34; 35]. From theoretical and experimental studies, the gas sensing properties of tungsten oxide films are strongly dependent on the relationship between film thickness, crystalline size and Debye length of electrons [12]. Tungsten oxide thin films obtained by electron beam evaporation and annealed in the temperature range of 350-800°C for 1-3 hours also indicated highly effective gas sensing properties to NO_2 [11].

The gas sensing properties of Ru implantation WO_3 thin films are not documented in the literature. Ruthenium does not oxidize easily and its oxides have different properties: conducting oxide (RuO_2) and oxidizing agents in organic compounds (RuO_4) [36]. It has been reported that doping of nanostructured thin SnO_2 films with Ru strongly enhanced the response toward gaseous NO_2 [37]. In this paper, the chemical and physical properties of various Ru-implanted tungsten oxide thin films have been characterized in order to understand the interaction between the Ru and the WO_3 on the nanoscale. Different techniques including Rutherford Back Scattering (RBS), Transmission Electron Microscope (TEM), Scanning Electron Microscope (SEM), X-Ray Photoelectron Spectroscopy (XPS) and Raman Spectroscopy have been used. In addition, we report the gas sensing characteristics of the films to NO and NO_2 by measuring the resistance change of the films during repeated exposure to the target gases.

2. Experimental

2.1 Sample preparation

Thin films of tungsten oxide were deposited on Si-substrate using thermal evaporation. Commercial powder of tungsten oxide (99.9% purity, average powder size 20 μm) was used for the evaporation. Single crystalline Si with about 300 nm SiO_2 top layer and interdigitated Pt electrodes printed on this layer (purchased form Electronics Design Center, Case Western Reserve University, Cleveland, USA) has been used as substrate. The effective area of the interdigitated electrodes was 8 mm x 8 mm. The electrode fingers had a line width and height of 100 μm and 300 nm, respectively. A bell jar type thermal evaporator unit (Varian Coater with Control System designed by AVT Pty Ltd, Australia) was used to deposit the WO_3 thin films. The substrate was placed at a distance of 38 cm in line of sight from the evaporation source. Deposition was carried out in high vacuum at 4 x 10^{-3} Pa with an evaporation rate of 35 nm/s. A quartz crystal film thickness monitor was used to achieve the desired thickness of the films. The WO_3 film sample preparation using thermal evaporation used in this experiment has been described in previous work [17].

Thin Solid Films; In Press Available online 11 March 2014,
http://dx.doi.org/10.1016/j.tsf.2014.02.084

These films were implanted with Ru using a direct extraction metal ion source, in a vacuum chamber, which was evacuated to a base pressure of about 3×10^{-4} Pa. After achieving the required vacuum, a high current was applied to the Ru cathode to generate a Ru ion beam that was accelerated at a voltage of 20 kV. The charge state distributions of Ru in the ions were: Ru^{+1}=0.4%; Ru^{+2}=17%; Ru^{+3}=75%; Ru^{+4}=7%; Ru^{+5}=0.6% with an average energy of about 60 keV and an average range of about 25 nm. Different Ru ion doses (10^{15} - $5x10^{17}cm^{-2}$) were obtained by varying the implantation time. Uniformity of the implantation was assured by sweeping the sample across the ion beam. After ion implantation, the films were annealed at 600°C for 2 hours in air to relieve the stress generated by ion implantation and improve the crystallinity of the films.

2.2 Sample characterization

RBS measurements were carried out to determine the concentration profile of Ru in the WO_3 films. A 1.8 MeV He^+ beam under a vacuum of 7×10^{-4} Pa was applied to the samples. The experimental data were fitted using SIMNRA software. The software is based on Microsoft Windows program and commonly applied for the simulation of backscattering spectra for ion beam analysis with MeV ions. A JEOL 1200 TEM was used at an accelerating voltage of 120 kV to investigate the cross-sectional area of the films in order to determine porosity, film thickness, and crystalline structure. During the TEM analysis, X-ray mapping has been applied to observe the distribution of the implanted Ru across the WO_3 film. The surface morphology and grain distribution of the films was obtained using a ZEISS SIGMA FE-SEM.

XPS analysis of the films were performed using Kratos AXIS Ultra XPS incorporating a 165 mm hemispherical electron energy analyzer, and using monochromatic Al K_α X-rays (1486.6 eV) at 150 W, incident at 45° to the sample surface. Photoelectron data were collected at a take-off angle of 90°. Survey scans were taken at analyzer pass energy of 160 eV and multiplex-high resolution scans at 20 eV. The survey scans were carried out over 1200 to 0 eV binding energy range with 1.0 eV steps and a dwell time of 100 ms, whereas narrow high-resolution scans were run with 0.05 eV steps and 250 ms dwell time. Base pressure in the analysis chamber was kept at 1.0×10^{-7} Pa and during sample analysis at 1.0×10^{-6} Pa. The bonding and crystal structure of the Ru-implanted WO_3 films were analyzed using a Renishaw System-1000 Raman spectroscopy. A HeNe laser excitation source of wavelength 633 nm with a 5 mW power at the sample was used. A Raman shift between the wavenumbers of 200 and 1200 cm^{-1} has been measured. A single crystal silicon wafer was used as a reference.

To monitor the gas-dependent resistances, the deposited Ru implanted WO_3 thin films were installed in a quartz-tube furnace with an inner diameter of 22 mm and 250°C and 350°C were selected as operating temperatures. The sensing properties of Ru implanted WO_3 were investigated in the presence of low concentration of NO and NO_2 target gases (0.25 - 2 ppm) in a 2 l/min gas flow of 20% O_2 balanced with N_2. The gas exchange time of the system is in the range of 7 s and the NO and NO_2 concentrations were validated by a Chemiluminescence

Thin Solid Films; In Press Available online 11 March 2014,
http://dx.doi.org/10.1016/j.tsf.2014.02.084

Detector (700 EL ht, Ecophysics, resolution 0.1 ppm). NO and NO_2 were applied alternately. A 2 ppm NO was added to the gas stream for 30 min followed by 30 min without NO, while periods with up to 2 ppm NO_2 lasted for 45 min followed by 75 min without NO_2.

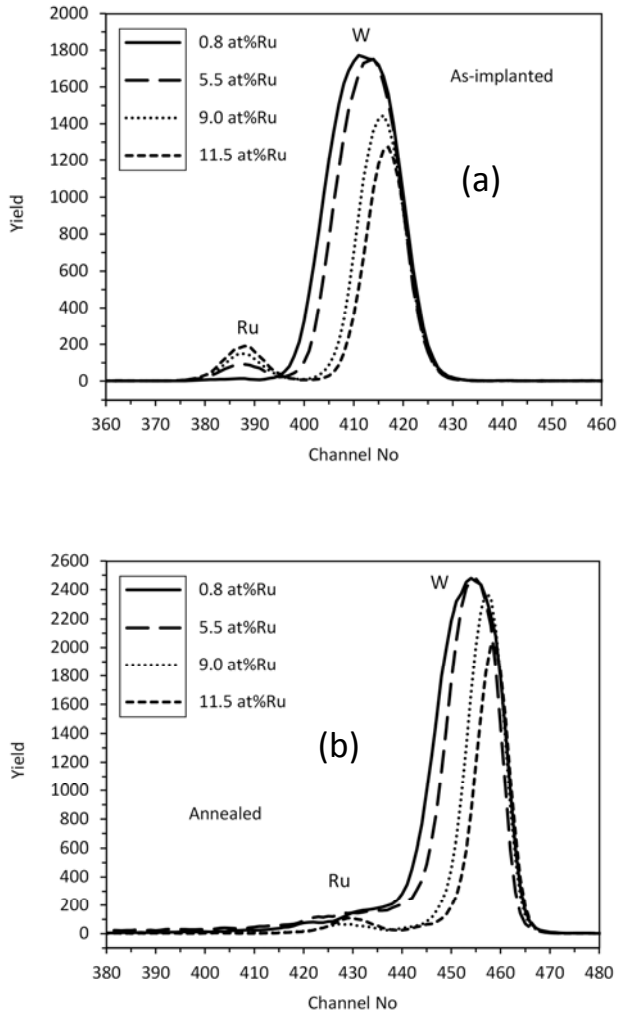

Figure 1: RBS spectra of four Ru-implanted tungsten oxide thin films of various Ru-concentrations (0.8-11.5 at% Ru): (a) before, and (b) after annealing at 600°C for 2 hours in air.

During exposure to NO and NO_2, the electrical impedance of the films was recorded time-continuously at an frequency of 10 Hz and an applied voltage (rms) of 0.1 V by an impedance analyzer (Alpha High Performance Frequency Analyzer, Novocontrol). The resistance R was calculated from the measured impedance applying an $R||C$ equivalent circuit model (resistance R in parallel to a capacitance C). The sensor response (R/R_0) and sensor dynamics (τ_{RESP} and τ_{REC}) were determined from the resistance curves. Prior to each measurement the samples were stabilized in 20% O_2 in N_2 at the particular operating temperature. If a stable signal was not achieved during a reasonable period of time, the samples were heated to 550°C to accelerate desorption of formerly adsorbed NO or NO_2 molecules. Further details of the test bench can be found in previous paper [38].

Thin Solid Films; In Press Available online 11 March 2014,
http://dx.doi.org/10.1016/j.tsf.2014.02.084

3. Results and Discussion

3.1. Film Behavior

We have performed RBS investigation of Ru-implanted tungsten oxide thin film samples before and after annealing at 600°C for 2 hours in air. Typical RBS spectra of the films with the presence of O, Si, Ru and W edges were observed. Figure 1a shows the W and Ru part of RBS spectra for four samples before annealing. The Ru to W intensity ratio increased with increasing Ru ion dose. The amounts of Ru concentration quantified by RBS in the four samples were 0.8, 5.5, 9 and 11.5 at%. As discussed in section 2.1, the average Ru ion-range calculated in WO_3 film was about 25 nm. This value is found to be similar to the results obtained using RBS depth analysis for Ru as shown in Table 1. Upon annealing the films, the W peak becomes sharper and more intense, whereas the Ru peak becomes broader as shown in Figure 1b. This broadening can be due to the inter-diffusion of the species into the un-implanted layer. From RBS depth profile analysis, the W and Ru appear to diffuse towards the film-substrate (SiO_2 layer) interface upon annealing. From Table 1, the diffusion is more pronounced in the low concentration sample as the film is more porous than the highly implanted samples. The Ru appears to penetrate almost through the whole film for the samples with 11.5 at % Ru.

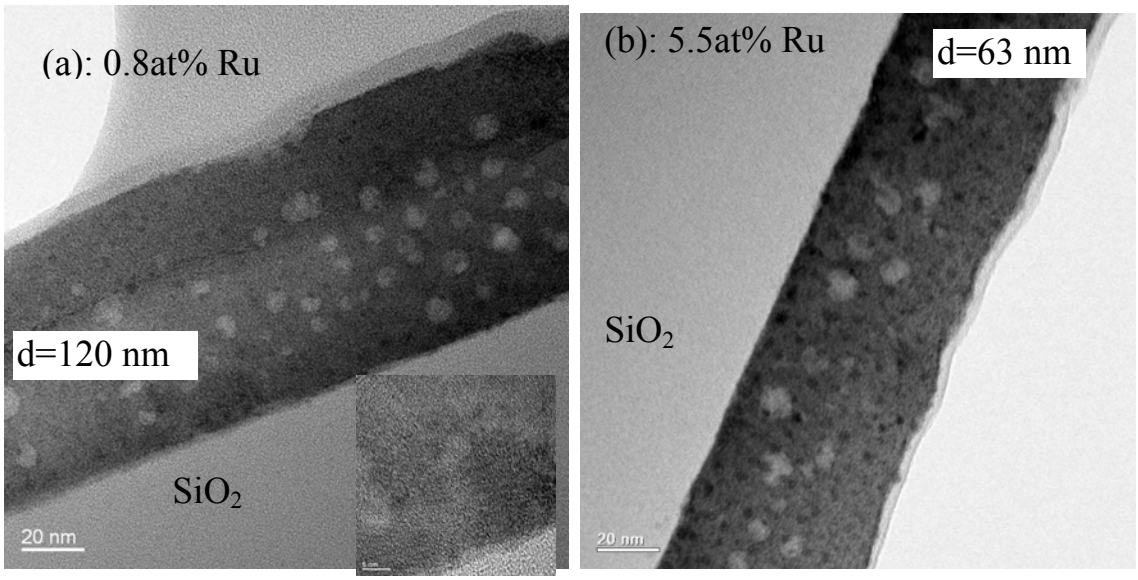

Thin Solid Films; In Press Available online 11 March 2014,
http://dx.doi.org/10.1016/j.tsf.2014.02.084

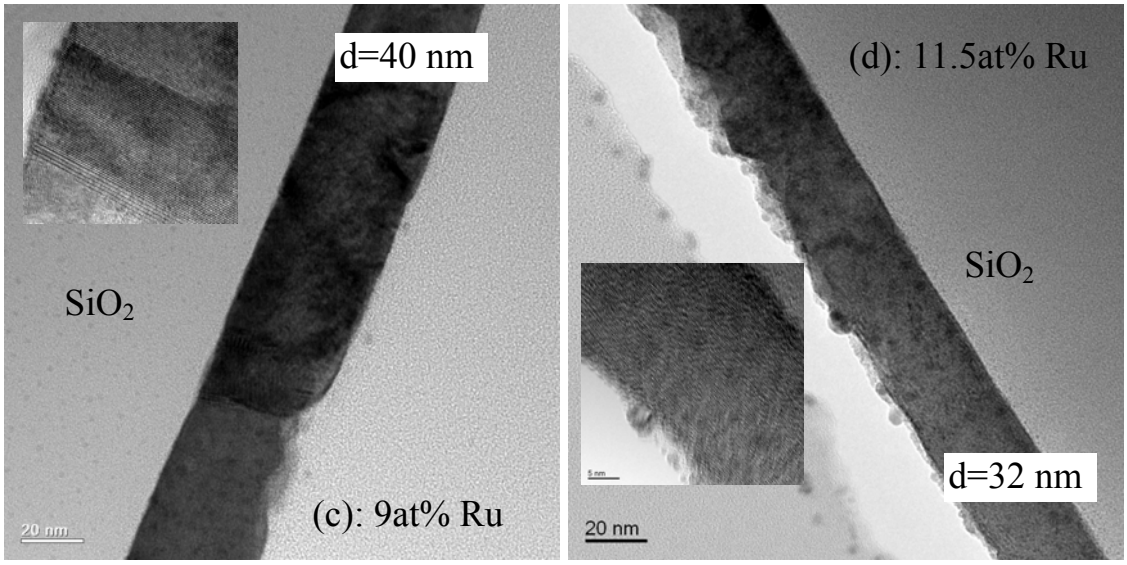

Figure 2 Cross-sectional TEM images of ion-implanted WO_3 films annealed at 600°C for 2 hours in air. The Ru-ion concentration of each film is (a) 0.8 at%, (b) 5.5 at%, (c) 9 at%, and (d) 11.5 at%. Insets show the high resolution of the films. Also, the thickness (d) of the films is shown.

Table 1: RBS depth analysis of Ru before and after annealing at 600°C for 2 hours in air.

Ru (at%)	Ru depth before annealing	Ru depth after annealing	Film Thickness
0.8	31 nm	41 nm	120 nm
5.5	28 nm	32 nm	63 nm
9	27 nm	27.5 nm	40 nm
11.5	27 nm	26.5 nm	32 nm

Figure 2 shows TEM cross-sectional images of the four annealed samples (0.8, 5.5, 9, 11.5 at% Ru). An amorphous interlayer of SiO_2 is also visible. Ruthenium was visible in the TEM X-ray mapping spectra in both the 9 at% Ru and 11.5 at% Ru samples. The presence of Ru in the 11.5 at% sample was in patches closer to the top-layer. No Ru was observed from the films with 0.8 at% Ru and 5.5 at% Ru concentrations. From Figure 1b, we expect a broad distribution of Ru in the film due to diffusion. This means that due to the detection limit of the X-ray mapping equipment, detection of the lightly implanted samples (0.8 and 5.5 at% Ru) was not possible. A porous film can be observed in the non-implanted region of the samples, with pore size distribution in the range of 5 to 15 nm. The films with lower implantation dose (i.e. 0.8 and 5.5 at% Ru) appeared to have two layers: an implanted top layer with reduced porosity and un-implanted bottom layer with average pore size of about 10 nm. However, a dense film with no porosity can be observed in the heavily implanted samples (i.e. 9 and 11.5 at% Ru). It can be observed from Figure 2, that the original thickness of the tungsten oxide film (d=120 nm) decreased with increasing Ru-ion dose. This can be due to high densification of the films when the irradiation time during implantation is increased. A shallow implanted layer of 25-35 nm in depth was observed in all the implanted films (TEM images in Figure 2) which is comparable to the Ru ion-range (25 nm) in WO_3

Thin Solid Films; In Press Available online 11 March 2014,
http://dx.doi.org/10.1016/j.tsf.2014.02.084

film obtained using charge states of Ru discussed in section 2.1. The high magnification of the samples (Figure 2 inset) shows that all the implanted films annealed at 600°C have some crystalline properties. Lattice planes are found in some regions indicating the presence of extremely tiny crystals of about 5 nm in size.

The density of the Ru-implanted WO_3 films has been calculated using the RBS and TEM results. As shown in Table 2, it was found to increase from 4.7 g/cm^3 for the lightly implanted film to 6.2 g/cm^3 for the film implanted with 11.5 at% Ru. The lightly implanted film shows a significant porosity. The density of pure WO_3 films obtained by thermal evaporation had been reported to vary between 5.0 to 6.5 g/cm^3 as the deposition temperature varies between RT and 280°C [39].

Table 2: Density of various Ru–implanted WO_3 films annealed at 600°C for 2 hours in air.

Concentration (at%)	RBS Thickness (at/cm^2)	TEM Thickness (nm)	Calculated Density (g/cm^3)
0.8	660x10^{15}	120	4.7
5.5	540x10^{15}	63	5.6
9	320x10^{15}	40	5.9
11.5	275x10^{15}	32	6.2

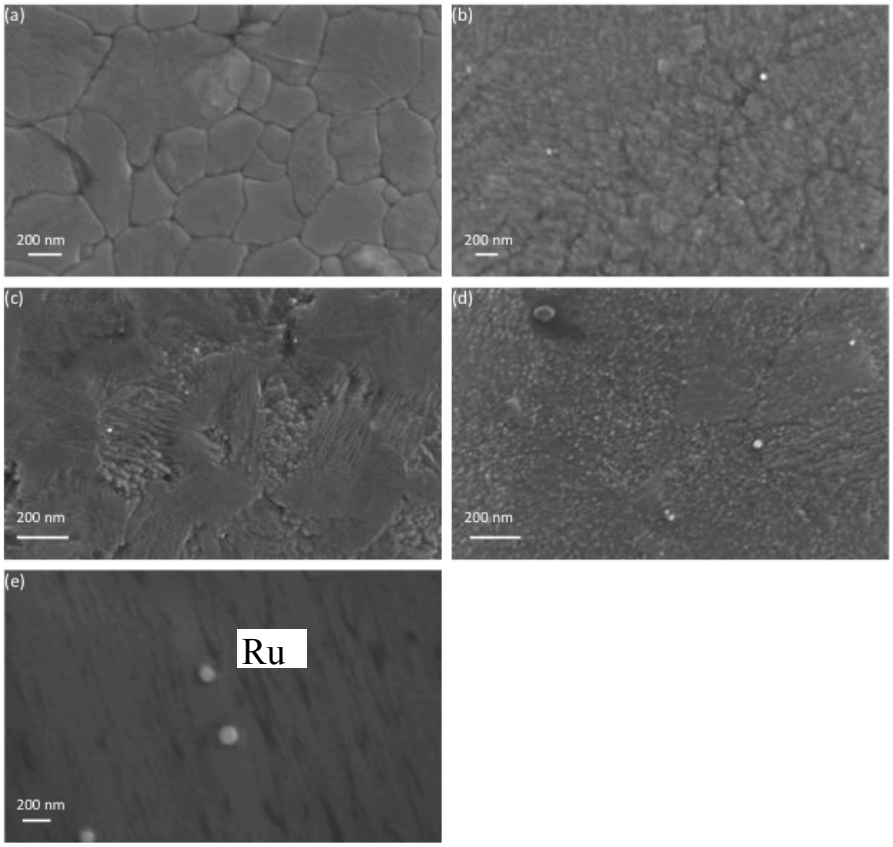

Figure 3 SEM images of pure and Ru-ion implanted WO_3 films. (a) un-implanted film (b) 0.8 at%, (c) 5.5 at%, (d) 9 at%, (e) 11.5 at% Ru-implanted films.

Thin Solid Films; In Press Available online 11 March 2014,
http://dx.doi.org/10.1016/j.tsf.2014.02.084

Figure 3 shows SEM micrographs of the pure and Ru-implanted WO_3 films annealed at 600°C for 2 hours in air. Figure 3a is a micrograph of the pristine film with crystalline grains separated by grain boundaries. Film defects created after Ru implantation were not removed completely after annealing the films. This can be revealed from the SEM images (Figures 3b-e) in which the remaining defects after annealing of the implanted films appeared higher in the films with higher ion doses. Fine nano-particles were grown on the surface of the films, most noticeably in the films with higher Ru concentrations. Energy Dispersive X-ray analysis reveals Ru on the surface of the sample with 11.5 at% Ru (Figure 3e). The higher Ru ion dose also caused densification of the films as observed by TEM in Figure 2.

Raman spectra of pristine and Ru-implanted WO_3 films annealed at 600°C in air are shown in Figure 4. The pristine film shows, four well known WO_3 peaks at 272, 329, 715, and 808 cm^{-1} and three Si bands at 303, 521, and 943 cm^{-1}. The Ru-implanted films show additional Raman bands at 408 and 451 cm^{-1}. The WO_3 peaks fall very close to the bands of the four strongest modes of monoclinic crystal structure of tungsten oxide [40]. The WO_3 peaks at 715 and 808 cm^{-1} are assigned to the O-W-O stretching vibration modes, whereas the peaks at 272 and 322 cm^{-1} can be attributed to the O-W-O bending modes. Raman bending modes are sensitive to local geometric distortion and the stretching modes due to defects resulting from substitutions or vacancies. The intensity and sharpness of the WO_3 bands decreases whereas the new bands associated with Ru increases with increasing concentration of Ru. It is interesting to observe that the 715 cm^{-1} band decreases strongly with respect to the 808 cm^{-1} peak. This indicates structural changes due to Ru ion implantation. In fact, both peaks (715 and 808 cm^{-1}) of the pure film are shifted to lower wavenumbers after Ru implantation (e.g. 711 and 800 cm^{-1}, respectively for the heavily implanted films), which is a hint for an increase of the W-O bond length due to the formation of defects and oxygen vacancies after the incorporation of Ru in the film. Oxygen vacancies repel W ions causing an increase in W-O bond length [41].

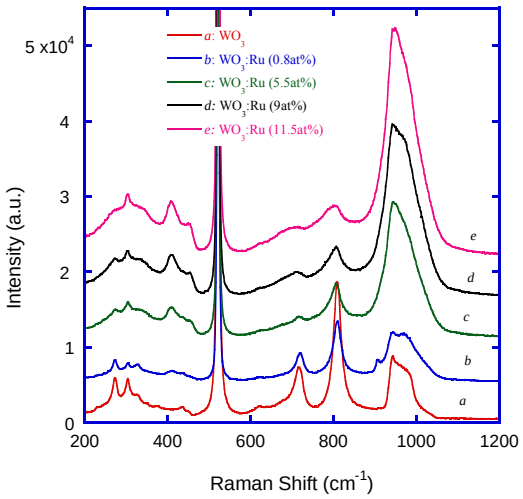

Figure 4 Raman spectra of as-deposited and Ru-implanted WO_3 films after annealing in air at 600°C for 2 hours

The Ru bands at 408 and 451 cm^{-1} are not attributed to the various oxidation states of RuO_x species because it is known that ruthenium does not oxidize easily [36]. Therefore, they can

be assigned to a metallic Ru band which is also confirmed by XPS analysis in Figure 5 although partial oxidation of Ru may not be excluded. This may be supported from the X-ray absorption spectroscopy study on Pd:SnO_2 layer in which Pd appeared to have metallic state at higher concentrations (3 wt%) and oxidized state at lower concentrations (0.2 wt%) [42]. Due to the relatively stronger band of Si at 943 cm^{-1}, it was not possible to verify the terminal W=O stretching bond (at about 952 cm^{-1}) at the surface and grain boundaries of the films [40]. However, the broadening of the band at 943 cm^{-1} with increasing Ru concentration indicates the presence of the terminal W=O stretching bond. The ratio of the integrated Raman intensity of W=O band to O-W-O stretching bands increases with increasing Ru concentration and this indicates that a higher number of defects (a larger surface area) were generated at higher implantation doses. This has been confirmed from the SEM images in Figure 3. The SEM images also showed tiny grains of Ru (nano-clusters of about 50 nm) on the surface of the film with the highest implantation dose (11.5 at% Ru).

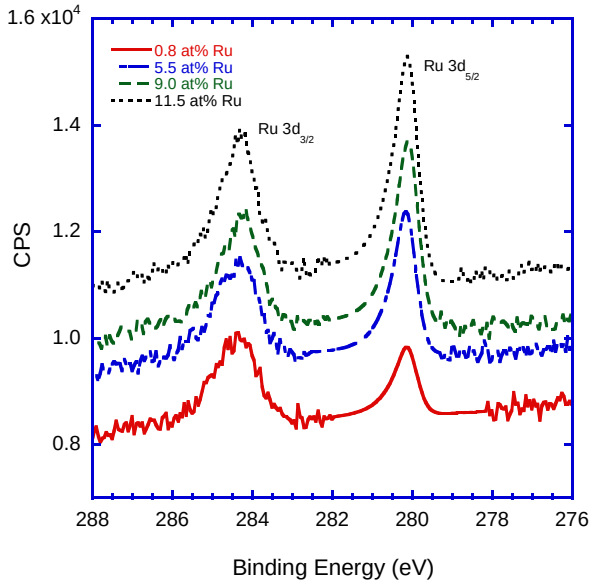

Figure 5 XPS spectra of Ru 3d of different concentrations in WO_3 films after annealing the films in air at 600°C for 2 hours.

Table 2: XPS peak positions of pure and Ru –implanted WO_3 films annealed at 600°C for 2 hours in air.

WO_3:Ru films	**Peak Position (eV)**	
	$Ru3d_{5/2}$	**Ru:W ratio**
0.8 at%Ru	280.14	1.59 at%
5.5 at%Ru	280.15	3.44 at%
9 at%Ru	280.16	4.73 at%
11.5 at%Ru	280.17	5.27 at%

Thin Solid Films; In Press Available online 11 March 2014,
http://dx.doi.org/10.1016/j.tsf.2014.02.084

XPS survey scans at the surface of lightly etched films show peaks of C, O, W and Ru. A high resolution scan of W at this surface shows peaks of W $4f_{7/5}$ (38.1 eV) and W $4f_{5/2}$ (35.8 eV) that are typical binding energies of WO_3 film. When the films are lightly etched, only peaks of C, O, W and Ru have been observed. Using the high resolution scans the peaks of Ru 3d have been analyzed (Figure 5). Due to the interference of the Ru $3d_{3/2}$ with C 1s peak at 284.4 eV, only the Ru $3d_{5/2}$ has been investigated using the metallic W $4f_{7/2}$ peak (31.40 eV) as a reference. The binding energy of Ru $3d_{5/2}$ for all the films is about 280.1 eV as shown in Table 3 and this peak position is similar to the previous reported values of metallic Ru [36; 43-45]. Assuming the peak position of Ru $3d_{3/2}$ coincides with that of C 1s, the estimated energy separation between the two Ru 3d peaks (Table 3) is similar to the reported value of 4.2 eV [44]. It can be seen from the Table that the peak position of Ru $3d_{5/2}$ remains almost the same when the Ru concentration is increased.

3.2. Gas Sensing Behavior

The sensing properties of Ru-implanted WO_3 films towards low concentrations of NO or NO_2 up to 2 ppm each were analyzed at 250°C and 350°C. The baseline resistance (R_0) of three implanted films (0.8, 5.5, 11.5 at% Ru) before being exposed to the target gases are shown in Table 4. The R_0 values increased only slightly with increasing Ru content at the operating temperature of 350°C. But the R_0 value of the film with 11.5 at% Ru is significantly larger than those of the films with lower Ru-concentrations at 250°C.

Table 4: Baseline resistance, R_0 (MΩ), response dynamics, τ_{RESP} and τ_{REC} (min) to 2 ppm NO_2 gas of three Ru-implanted WO_3 films annealed at 600°C for 2 hours in air.

	Operating Temperature 250°C			Operating Temperature 350°C		
WO_3:Ru	R_0 (MΩ)	τ_{RESP} (2 ppm)	τ_{REC} (2 ppm)	R_0 (MΩ)	τ_{RESP} (2 ppm)	τ_{REC} (2 ppm)
0.8 at%	0.42	45 min	68 min	0.26	36 min	71 min
5.5 at%	0.44	21 min	72 min	0.32	41	82 min
11.5 at%	3.58	36 min	72 min	0.41	43	71 min

Figure 6a shows the dynamic response of the films with 0.8, 5.5 and 11.5 at% Ru exposed to 0.25 to 2 ppm NO_2 alternated with 2 ppm NO at an operating temperature of 350°C. The NO_x concentration (left axis) reflects the sum of NO and NO_2 measured by the CLD located downstream of the samples. According to the sensing mechanism of n-type semiconductors the resistance R and hence the related sensor response R/R_0 of all investigated films increases in the presence of the oxidizing gases NO and NO_2. During the NO_2 periods of 45 min, R/R_0 of all samples increases progressively without reaching a steady state value. Additionally, R/R_0 is not fully recovering during the following 75 min without NO or NO_2. The response

Thin Solid Films; In Press Available online 11 March 2014,
http://dx.doi.org/10.1016/j.tsf.2014.02.084

and recovery times τ_{RESP} and τ_{REC} given in Table 4 are obtained from Figure 6. While the sample with 5.5 at% Ru did not respond to NO, the sensor response (R/R_0) of the 0.8 at% Ru and 11.5 at% Ru increases instantaneously upon introduction of NO with a smaller signal compared to NO_2 but then decreases as continuing the trend of the period without NO or NO_2. During the first NO dosing step, some of the NO in the gas stream was oxidized to NO_2 resulting in a distortion of the sensor response since the resistance depends differently on NO and NO_2. The results indicate that the response of the films with Ru concentration of 0.8 and 11.5 at% are significantly higher at 350°C compared to those of the film with 5.5 at% Ru. From the above results, there is no clear correlation between the Ru amount and the gas sensor performance. This can be due to the change of other film parameters (e.g. film porosity and thickness) due to implantation. From TEM in Figure 2, the film with the lowest Ru concentration (0.8 at%) is porous and shows higher sensor response. While there is no film porosity in the sample with 11.5 at% Ru, its sensing response was almost similar to the 0.8 at% Ru porous film and this is primarily caused by the metallic Ru clusters as adsorption surface sites [46]. However, bulk sensitization effect due to higher amount of film defects can be a possible additional sensing mechanism at this temperature. The sample with moderate amount of Ru (i.e. 5.5 at% Ru) shows the lowest response and the slowest sensor dynamics (highest response and recovery times), mainly due to presumably reduced film porosity at the surface of the film.

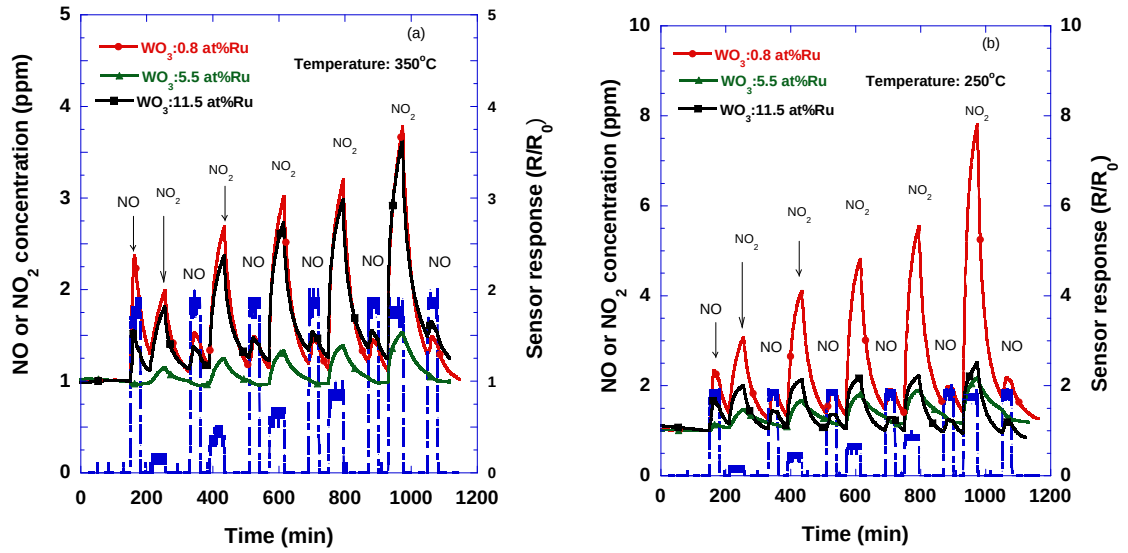

Figure 6 Dynamic normalized resistance curve R/R_0 of Ru-implanted WO_3 thin films annealed at 600°C for 2 hours in air upon exposure to various concentrations of NO_2 and NO target gases in 20 % O_2 balanced with N_2 at operating temperatures of (a) 350°C and (b) 250°C.

The sensor response of the lightly implanted WO_3 film (0.8 at% Ru) is almost doubled when the operating temperature is lowered from 350°C to 250°C (Figure 6b). This is expected as it is known that pure WO_3 film shows better response at lower operating temperatures [16-19; 35]. At 250°C, the baseline resistance of the heavily implanted WO_3 film (11.5 at% Ru) is

significantly higher and has therefore a lower sensor response (Figure 6b). Conduction in films with defects can be temperature dependent and hence the film with 11.5 at% Ru have higher amount of defects and appeared to have significantly higher baseline resistance at lower temperature (250^{o}C). Table 4 shows the dynamics (response and recover times) of the three sensors to 2 ppm NO_2 at 250^{o}C and 350^{o}C. From these results one may conclude that an increasing Ru concentration improves the sensor response. But poor sensing properties can be anticipated when the film porosity has been reduced. In addition, ion implantation helps to form defects and oxygen vacancies that can enhance the sensor response. It is concluded that addition of Ru into WO_3 films with sufficient film porosity and film thickness can be beneficial for NO_x sensing.

4. Conclusions

Different amounts of Ru were introduced into thermally evaporated WO_3 films by ion implantation and subsequently annealed at 600^{o}C for 2 hours in air. The Ru concentrations of four samples have been quantified by RBS as 0.8 at%, 5.5. at%, 9 at% and 11.5 at%. RBS depth profile indicated that the Ru in the annealed samples uniformly diffuse towards the film-substrate interface. The film thicknesses and porosity of these samples were found to decrease with increasing Ru-ion dose due to densification of the films as observed by TEM and SEM. From Raman spectroscopy all the films have shown typical vibrational peaks of the Monoclinic WO_3 phase, and two additional peaks at 408 and 451 cm^{-1} that are associated with metallic Ru. A large amount of oxygen vacancies and defects (i.e. a larger surface area) were generated at higher Ru implantation doses as analyzed from the integrated Raman intensity which is important for gas sensing. The SEM also indicated an increased amount of defects with higher implantation doses which supported the observation from the Raman spectra. In addition tiny grains of Ru (nano-clusters of about 50 nm) have been observed in the heavily implanted films. XPS showed that a metallic state of Ru in the WO_3 films and the peak positions of Ru (280.1 eV) was not shifted by the change of Ru concentration. The results indicated that the incorporation of Ru into WO_3 films have formed unique structure and properties as compared to the pure WO_3 film.

The gas sensing properties of the Ru-implanted films towards NO_2 and NO gases in the concentration range of 0.25-2 ppm at operating temperature of 250^{o}C and 350^{o}C have been performed. While the reduction of film porosity and film thickness had negative effect on the sensing performance, the increasing amount of Ru concentration has shown a crucial role in enhancing the sensor response to NO_2 gas. From the measurements, the sensor response of the heavily implanted sample (11.5 at% Ru) at higher temperature (350^{o}C) has almost similar value to the 0.8 at% Ru porous film and this is predominately due to the metallic Ru clusters acting as additional adsorption surface sites and the amount of defects created by ion implantation but this enhancement was not observed at 250^{o}C. This experiment proves that the sensor with lightly implanted film (i.e. 0.8 at% Ru) having significant film porosity and thickness was found to have the highest sensing performance to NO_2 in the measured operating temperature of 250^{o}C and 350^{o}C.

Thin Solid Films; In Press Available online 11 March 2014,
http://dx.doi.org/10.1016/j.tsf.2014.02.084

Acknowledgements

The authors acknowledge Australian Institute of Nuclear Science and Engineering for providing support to use the facility (Ion Implanter, RBS and TEM) at the Australian Nuclear Science and Technology Organisation. The Central Analytical Research Facility at QUT is also acknowledged for supporting us to use their SEM.

References

[1] A. Dieguez, A. Romano-Rodriguez, J.R. Morante, U. Weimar, M. Schweizer-Berberich, W. Gopel, Morphological analysis of nanocrystalline SnO2 for gas sensor applications, Sens. Actuators B Chem 31 (1996) 1-8.

[2] X. He, J. Li, X. Gao, L. Wang, NO2 sensing characteristics of WO3 thin film microgas sensor, Sens. Actuators B Chem 93 (2003) 463-467.

[3] V. Khatko, E. Llobet, X. Vilanova, J. Brezmes, J. Hubalek, K. Malysz, X. Correig, Gas sensing properties of nanoparticle indium-doped WO3 thick films, Sens. Actuators B Chem 111-112 (2005) 45-51.

[4] T. Pagnier, M. Boulova, A. Galerie, A. Gaskov, G. Lucazeau, Reactivity of SnO2-CuO nanocrystalline materials with H2S: a coupled electrical and Raman spectroscopic study, Sens. Actuators B Chem 71 (2000) 134-139.

[5] B. Fruhberger, M. Grunze, D.J. Dwyer, Surface chemistry of H2S-sensitive tungsten oxide films, Sens. Actuators B Chem 31 (1996) 167-174.

[6] I. Jimenez, J. Arbiol, G. Dezanneau, A. Cornet, J.R. Morante, Crystalline structure, defects and gas sensor response to NO2 and H2S of tungsten trioxide nanopowders, Sens. Actuators B Chem 93 (2003) 475-485.

[7] G. Sarala Devi, V. Bala Subrahmanyam, S.C. Gadkari, S.K. Gupta, NH3 gas sensing properties of nanocrystalline ZnO based thick films, Anal. Chim. Acta 568 (2006) 41-46.

[8] K. Zakrzewska, Gas sensing mechanism of TiO2-based thin films, Vacuum 74 (2004) 335-338.

[9] N. Koshizaki, T. Oyama, Sensing characteristics of ZnO-based NOx sensor, Sens. Actuators B Chem 66 (2000) 119-121.

[10] A. Rothschild, Y. Komem, The effect of grain size on the sensitivity of nanocrystalline metal-oxide gas sensors, J. App. Phys. 95 (2004) 6374-6380.

[11] O. Berger, W.-J. Fischer, V. Melev, Tungsten-oxide thin films as novel materials with high sensitivity and selectivity to NO2, O3 and H2S. Part I: Preparation and microstructural characterization of the tungsten-oxide thin films, J. Mater. Sci.: Mater. Elect. 15 (2004) 463-482.

[12] O. Berger, T. Hoffmann, W.-J. Fischer, V. Melev, Tungsten-oxide thin films as novel materials with high sensitivity and selectivity to NO2, O3, and H2S. Part II: Application as gas sensors, J. Mater. Sci: Mater. Elect. 15 (2004) 483-493.

[13] N. Barsan, D. Koziej, U. Weimar, Metal oxide-based gas sensor research: How to?, Sens. Actuators B Chem 121 (2007) 18-35.

[14] E. Comini, M. Ferroni, V. Guidi, A. Vomiero, P.G. Merli, V. Morandi, M. Sacerdoti, G.D. Mea, G. Sberveglieri, Effects of Ta/Nb-doping on titania-based thin films for gas-sensing, Sens. Actuators B Chem 108 (2005) 21-28.

[15] V. Guidi, D. Boscarino, E. Comini, G. Faglia, M. Ferroni, C. Malagu, G. Martinelli, V. Rigato, G. Sberveglieri, Preparation and characterisation of titanium-tungsten sensors, Sens. Actuators B Chem 65 (2000) 264-266.

[16] M. Ahsan, M.Z. Ahmad, T. Tesfamichael, J. Bell, W. Wlodarski, N. Motta, Low temperature response of nanostructured tungsten oxide thin films toward hydrogen and ethanol, Sens. Actuators B Chem 173 (2012) 789-796.

[17] M. Ahsan, T. Tesfamichael, M. Ionescu, J. Bell, N. Motta, Low temperature CO sensitive nanostructured WO3 thin films doped with Fe, Sens. Actuators B Chem 162 (2012) 14-21.

Thin Solid Films; In Press Available online 11 March 2014,
http://dx.doi.org/10.1016/j.tsf.2014.02.084

[18] T. Tesfamichael, M. Arita, T. Bostrom, J.M. Bell, Thin Film Deposition and Characterization of Pure and Iron-Doped Electron-Beam Evaporated Tungsten Oxide for Gas Sensors, Thin Solid Films 518 (2010) 4791–4797.
[19] T. Tesfamichael, A. Ponzoni, M. Ahsan, G. Faglia, Gas sensing characteristics of Fe-doped tungsten oxide thin films, Sens. Actuators B Chem 168 (2012) 345-353.
[20] M.A. Ponce, C.M. Aldao, M.S. Castro, Influence of particle size on the conductance of SnO2 thick films, J. Eur. Ceram. Soc. 23 (2003) 2105-2111.
[21] X. Wang, S.S. Yee, W.P. Carey, Transition between neck-controlled and grain-boundary-controlled sensitivity of metal-oxide gas sensors, Sens. Actuators B Chem 25 (1995) 454-457.
[22] F. Rettig, R. Moos, Morphology dependence of thermopower and resistance in semiconducting oxides with space charge regions, Solid State Ionics 179 (2008) 2299-2307.
[23] R. Artzi-Gerlitz, K.D. Benkstein, D.L. Lahr, J.L. Hertz, C.B. Montgomery, J.E. Bonevich, S. Semancik, M.J. Tarlov, Fabrication and gas sensing performance of parallel assemblies of metal oxide nanotubes supported by porous aluminum oxide membranes, Sens. Actuators B Chem 136 (2009) 257-264.
[24] K. Zakrzewska, Mixed oxides as gas sensors, Thin Solid Films 391 (2001) 229-238.
[25] N. Han, L. Chai, Q. Wang, Y. Tian, P. Deng, Y. Chen, Evaluating the doping effect of Fe, Ti and Sn on gas sensing property of ZnO, Sens. Actuators B Chem 147 (2010) 525-530.
[26] A. Hoel, L.F. Reyes, P. Heszler, V. Lantto, C.G. Granqvist, Nanomaterials for environmental applications: novel WO3-based gas sensors made by advanced gas deposition, Curr. Appl. Phys. 4 (2004) 547-553.
[27] A. Tricoli, M. Righettoni, A. Teleki, Semiconductor Gas Sensors: Dry Synthesis and Application, Angew. Chem. Int. Ed. 49 (2010) 7632–7659.
[28] A. Roldan, M. Boronat, A. Corma, F. Illas, Theoretical confirmation of the enhanced facility to increase oxygen vacancy concentration in TiO_2 by iron doping, J. Phys. Chem. C 114 (2010) 6511–6517.
[29] H. Kawasaki, T. Ueda, Y. Suda, T. Ohshima, Properties of metal doped tungsten oxide thin films for NOx gas sensors grown by PLD method combined with sputtering process, Sens. Actuators B Chem 100 (2004) 266-269.
[30] A. Boudiba, C. Zhang, C. Navio, C. Bittencourt, R. Snyders, M. Debliquy, Preparation of highly selective, sensitive and stable hydrogen sensors based on Pd-doped tungsten trioxide, Procedia Eng. 5 (2010) 180-183.
[31] M. Stankova, X. Vilanova, J. Calderer, E. Llobet, J. Brezmes, I. Gràcia, C. Cané, X. Correig, Sensitivity and selectivity improvement of rf sputtered WO3 microhotplate gas sensors, Sens. Actuators B Chem 113 (2006) 241-248.
[32] E. Rossinyol, A. Prim, E. Pellicer, J. Rodríguez, F. Peiró, A. Cornet, J.R. Morante, B. Tian, T. Bo, D. Zhao, Mesostructured pure and copper-catalyzed tungsten oxide for NO2 detection, Sens. Actuators B Chem 126 (2007) 18-23.
[33] E. Comini, L. Pandolfi, S. Kaciulis, G. Faglia, G. Sberveglieri, Correlation between atomic composition and gas sensing properties in tungsten-iron oxide thin films, Sens. Actuators B Chem 127 (2007) 22-28.
[34] G.G. Mandayo, E. Castaño, F.J. Gracia, A. Cirera, A. Cornet, J.R. Morante, Strategies to enhance the carbon monoxide sensitivity of tin oxide thin films, Sens. Actuators B Chem 95 (2003) 90-96.
[35] M. Penza, M.A. Tagliente, L. Mirenghi, C. Gerardi, C. Martucci, G. Cassano, Tungsten trioxide (WO3) sputtered thin films for a NOx gas sensor, Sens. Actuators B Chem 50 (1998) 9-18.
[36] H.Y.H. Chan, C.G. Takoudis, M.J. Weaver, High-Pressure Oxidation of Ruthenium as Probed by Surface-Enhanced Raman and X-Ray Photoelectron Spectroscopies, J. Catal. 172 (1997) 336-345.
[37] O.V. Safonova, G. Delabouglise, B. Chenevier, A.M. Gaskov, M. Labeau, CO and NO2 gas sensitivity of nanocrystalline tin dioxide thin films doped with Pd, Ru and Rh, Mater. Sci. Eng., C 21 (2002) 105-111.
[38] A. Groß, G. Beulertz, I. Marr, D.J. Kubinski, J.H. Visser, R. Moos, Sensors 12 (2012) 2831-2850.
[39] M.C. Rao, O.M. Hussain, Growth and Characterization of Vacuum Evaporated WO3 Thin Films for Electrochromic Device Application, Res. J. Chem. Sci. 7 (2011) 92-95.
[40] T. Siciliano, A. Tepore, G. Micocci, A. Serra, D. Manno, E. Filippo, WO3 gas sensors prepared by thermal oxidization of tungsten, Sens. Actuators B Chem 133 (2008) 321-326.

Thin Solid Films; In Press Available online 11 March 2014,
http://dx.doi.org/10.1016/j.tsf.2014.02.084

[41] S. Keshri, A. Kumar, D. Kabiraj, Tailoring of optical and gas sensitivity behaviors of WO3 films by low energy Ar+ ion implantation, Thin Solid Films 526 (2012) 50-58.
[42] D. Koziej, M. Hübner, N. Barsan, U. Weimar, M. Sikorazc, J.-D. Grunwaldt, Operando X-ray absorption spectroscopy studies on Pd-SnO2 based sensors, Phys. Chem. Chem. Phys. 11 (2009) 8620-8625.
[43] J.S. Shaikh, R.C. Pawar, R.S. Devan, Y.R. Ma, P.P. Salvi, S.S. Kolekar, P.S. Patil, Synthesis and characterization of Ru doped CuO thin films for supercapacitor based on Bronsted acidic ionic liquid, Electrochim. Acta 56 (2011) 2127-2134.
[44] D. Rochefort, P. Dabo, D. Guay, P.M.A. Sherwood, XPS investigations of thermally prepared RuO2 electrodes in reductive conditions, Electrochim. Acta 48 (2003) 4245-4252.
[45] C. Mun, J.J. Ehrhardt, J. Lambert, C. Madic, XPS investigations of ruthenium deposited onto representative inner surfaces of nuclear reactor containment buildings, Appl. Surf. Sci. 253 (2007) 7613-7621.
[46] M. Hübner, D. Koziej, M. Bauer, N. Barsan, K. Kvashnina, M.D. Rossell, U. Weimar, J.-D. Grunwaldt, The Structure and Behavior of Platinum in SnO2-Based Sensors under Working Conditions, Angew. Chem. Int. Ed. 50 (2011) 2841-2844.